JTTEE5 19:1294–1300
DOI: 10.1007/s11666-010-9524-x
1059-9630/$19.00 © ASM International

Technical Note

Microstructure and Thermal Properties of Nanostructured 4 wt.%Al_2O_3-YSZ Coatings Produced by Atmospheric Plasma Spraying

Qinghe Yu, Abdul Rauf, and Chungen Zhou

(Submitted March 18, 2010; in revised form May 23, 2010)

Microstructure and phase composition of the nanostructured Al_2O_3 doped YSZ coatings by atmospheric plasma spraying method have been characterized with XRD, TEM and SEM. The nanostructured 4AlYSZ coatings consist mainly of t-ZrO_2, crystalline Al_2O_3 phase is absent in the coatings and the grain size of the 4AlYSZ coating is about 65 nm. The APS 4AlYSZ coating is characterized by nanozones, dense area and voids. After doping, the coefficient of thermal expansion of YSZ is decreased to 10.928×10^{-6}/K. The addition of Al_2O_3 has a great influence on decreasing the thermal conductivity of nano-YSZ, which is mainly caused by the point defect scattering and grain-boundary scattering. The lifetime of nanostructured 4AlYSZ coating is about 1000 cycles at 1100 °C.

Keywords atmospheric plasma spraying, nanostructured Al_2O_3-Y_2O_3-ZrO_2, thermal barrier coatings, thermal conductivity, thermal cycling life

1. Introduction

Nanostructured yttria stabilized zirconia coatings (nano-YSZ) have received widely interest because of their low thermal conductivity, high coefficient of thermal expansion, excellent thermodynamic and mechanical properties toward thermal cycling in the turbine environment (Ref 1-7). However, the grain growth and the phase instability during annealing (Ref 4, 5, 8, 9), and consequently the disappearance of the nanostructure during sintering process, severely weaken the thermal and mechanical properties of the coatings. In order to improve the thermal and mechanical properties, nanostructrued coatings have been modified by doping with several additives, such as Al_2O_3, La_2O_3 and HfO_2 (Ref 6, 10-18). Zhou and coworkers (Ref 11) investigated thermal stability of nanostructured Al_2O_3-YSZ coatings prepared by air plasma spray method. The results showed that adding alumina into the zirconia is effective in inhibiting the grain growth of nanostructured YSZ thermal barrier coatings. The mechanism on inhibiting the grain growth of nanostructured YSZ thermal barrier coatings has been discussed in detail. The effect of small amount of La_2O_3 (Ref 19-23) additions on thermal conductivity, structural stability is investigated. The addition of a small quantity of La_2O_3 (Ref 13, 14, 19) is effective in improving the sintering resistance and lowering the thermal conductivity of traditional YSZ produced by air plasma spray. However, the reports about thermal properties of nanostructured Al_2O_3-YSZ coatings prepared by air plasma spray method are limited.

With the above background, the present study deals with a plasma sprayed nanostructured YSZ coating with an addition of nano-Al_2O_3 particles. Microstructure and thermal properties of the coating have been investigated. The mechanism on decreasing the thermal conductivity by doped Al_2O_3 was discussed through the relationships among the point defect scattering, grain-boundary scattering and thermal conductivity.

Qinghe Yu, Abdul Rauf, and **Chungen Zhou**, Key Laboratory of Aerospace Materials and Performance (Ministry of Education), Department of Materials Science and Engineering, Beijing University of Aeronautics and Astronautics, Beijing 100191, China. Contact e-mail: cgzhou@buaa.edu.cn.

2. Experimental Procedure

2.1 Preparation of the Nanostructured 4 wt.%Al_2O_3-8 wt.%Y_2O_3-ZrO_2 Coating

The original 4 wt.%Al_2O_3-8 wt.%Y_2O_3-ZrO_2 (4AlYSZ) powder is composed of nanostructured 8 wt.%Y_2O_3-ZrO_2 (YSZ) and Al_2O_3 (Nanjing high technology nano company of China). The average size of YSZ and Al_2O_3 particle is 30 and 20 nm respectively. The individual nanoparticle is so fine that cannot be used for plasma spray. Before spraying finely dispersed particles must be agglomerated to size about 30-70 μm. Suspensions for spray-drying were made by mixing nano-Al_2O_3 and nano-YSZ powders with acaciagum and ammonium citrate, then ball-milling for more than 24 h. The amount of acaciagum binder introduced in the slurry was fixed at 2 wt.% whereas the quantity of ammonium citrate was about 1 wt.% (Ref 24). After that the suspension was pumped into the drying chamber, it was separated into small droplets immediately by the compressed feeding gas. Afterwards, the droplet shrank because of the fast evaporation of solvent. At the end of the drying period, the dried granules were collected and sieved to get the powders suitable for plasma spraying. The main controlled operating parameters were the air temperature at the entry (220 °C), at the exit (140 °C) and inside the chamber (180 °C) (Ref 25). A particle size distribution around 50 μm was used in this study.

The 4 wt.%Al_2O_3-8 wt.%Y_2O_3-ZrO_2 powder was sprayed on the stainless steel for thermal diffusivity measurements. The parameters for plasma spraying have been reported in our previous study (Ref 8). The temperature of the substrate and coating during the plasma spraying was about 300-400 °C because of air cooling. The coating was detached from the stainless steel, and was 12.6 mm in diameter and 1 mm in thickness.

For thermal cycling test, the substrates were cut into coupons with a dimension of 15 mm × 10 mm × 3 mm from a wrought sheet of nickel-based superalloy with nominal composition (wt.%) of Ni-5Co-10Cr-4Mo-5W-3.5Al-2Ti-2Nb (K3). In order to improve the adherence of the coating, these coupons were grit-blasted, using 250-μm alumina grit, to obtain a sharp-peaked surface contour with a roughness average of 4-5 μm. The coupons were coated with a NiCrAlY bond coat to a thickness of about 100 μm. A top coat of nano-4AlYSZ was deposited on the substrate to a thickness of about 200 μm using APS process. For comparison, the nanostructured and conventional YSZ coating with the same thicknesses of bond coat and ceramic layer as that of nanostructured AlYSZ coating were produced under the same plasma spraying parameters.

2.2 Thermal Conductivity Measurement

Thermal diffusivity measurements have been carried out by using the laser flash technique (LFA427, NETZSCH). This method consists of heating the front face of a sample (typically a small disk-shaped specimen) by a short laser detecting temperature rise on its rear surface by an infrared detector. For evaluating the thermal diffusivity, the solution proposed originally by Parker et al. (Ref 26) consisted of using the following relation

$$\alpha = 0.1388\frac{L^2}{t_{1/2}} \quad \text{(Eq 1)}$$

where $t_{1/2}$ and L are the time corresponding to the half-maximum increase of the temperature and the sample thickness. Both sides of the laser flash specimens were coated with graphite to make them opaque to the laser used for heating. Three measurements of thermal diffusivity were taken for each sample at each temperature and averaged. At least three replicates for each testing condition were performed.

The thermal conductivity of each sample was calculated using the following equation:

$$k = \alpha \times C_p \times \rho \quad \text{(Eq 2)}$$

where k is the stands for thermal conductivity, α the thermal diffusivity, C_p the heat capacity and ρ is the bulk density of the material. Density was assumed constant.

2.3 Sintering and Thermal Cycling Life Test

Shrinkage of the specimens at 1200 °C for 12 h was determined using a high temperature dilatometer (Netzsch DIL 402E, Germany) on specimens of 25 mm in length and 5 mm in both width and height.

The specimens were kept in furnace at 1100 °C for 50 min and cooled in air for 5 min as a cycle. The lifetime of the coatings were defined by the number of cycles at which 5% of total coating surface area is spalled or delaminated.

2.4 Structural Analysis of the Nanostructured AlYSZ Coating

The original zirconia powders and the as-sprayed coatings were characterized using a D/max 2200pc x-ray diffractometer (Cu Kα radiation; Rigaku, Tokyo, Japan). The microstructure of the coatings was determined by an S-3500 scanning electron microscope (SEM, Hitachi, Tokyo, Japan). Particle morphology observation and crystal structure determination were also performed on an analytical Transmission Electron Microscope (TEM).

3. Results

3.1 Phase Analysis

Figure 1 illustrates the XRD patterns of plasma sprayed 4 wt.%Al_2O_3-YSZ coatings. From Fig. 1, the as-sprayed 4AlYSZ coating is mainly composed of t-ZrO_2

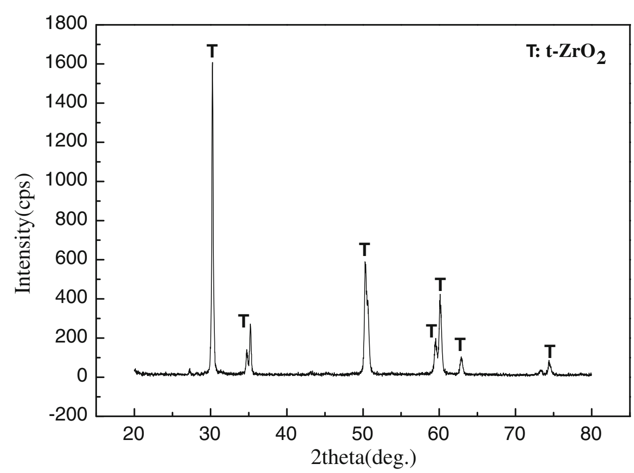

Fig. 1 The XRD patterns of plasma sprayed nanostructured 4 wt.%Al_2O_3-YSZ coating

phase. The nontransformable t phase in ZrO_2 existed as the nonequilibrium t′ phase, which was formed due to quenching of droplet after impacting on the substrate during plasma spraying. No m-ZrO_2 or α-Al_2O_3 phase appears after plasma spraying. The absence of α-Al_2O_3 can be explained by the solid solution of Al atoms in ZrO_2 during plasma spraying (Ref 11). All Al_2O_3 is dissolved in ZrO_2 and no YAG oxides are formed. According to the phase diagram, the Al_2O_3 reacts with Y_2O_3 to form YAG at the high temperature but needs a long reacting time. Plasma spraying is such a fast cooling process that the elements can not be diffused. Therefore, no YAG can be formed. It has been proved by the SADEPs in our previous work (Ref 11).The similar results have been found in Ref 5 and 27.

The mean grain sizes of coatings are calculated using the Scherrer equation (Ref 28, 29)

$$B_p(2\theta) = \frac{0.9\lambda}{D\cos\theta} \qquad \text{(Eq 3)}$$

where D is the average dimension of crystallite, B_p (2θ) the broadening of the diffraction line measured at the half maximum intensity, λ (0.154 nm) and θ denotes the wavelength of the x-rays and the Bragg diffraction angle, respectively. The correction for instrumental broadening is taken into consideration in the measurement of the peak broadening by comparing the widths at half maximum intensity of x-ray reflection between the sample and the single crystalline Si standard, and then Gaussian correction is used to remove the instrumental broadening to obtain the true crystal broadening.

$$B_p^2(2\theta) = B_h^2(2\theta) - B_f^2(2\theta) \qquad \text{(Eq 4)}$$

where $B_p(2\theta)$ is the true half maximum width; $B_h(2\theta)$ and $B_f(2\theta)$ are the half maximum widths of the sample and the single crystalline Si standard, respectively (Ref 30).

Corresponding to Fig. 1, the average grain size of the as-sprayed 4AlYSZ coating calculated by Eq 3 is about 65 nm.

3.2 Microstructure of As-Sprayed Nanostructured 4AlYSZ Coating

The fractured cross-section morphology of the as-sprayed nanostructured 4AlYSZ coating is shown in Fig. 2. The APS coating is characterized by nanozones, dense area, voids (Fig. 2). The dense area is comprised of melted particles while the loose structure contains the equiaxed grains and nanosized grains formed by partially melted and unmelted particles. This characteristic of the microstructure is beneficial to enhance the phonon scattering by the nano-particles, voids and microcracks (Ref 31).

Figure 3 shows the polished cross section of as-sprayed nanostructured 4AlYSZ. As shown in Fig. 3, the observed microstructure is typical of APS nanostructured coatings with nanozones (unmelted or partially melted particles), splats, microcracks and high volume spheroidal pores. Figure 4 is the TEM image of the as-sprayed

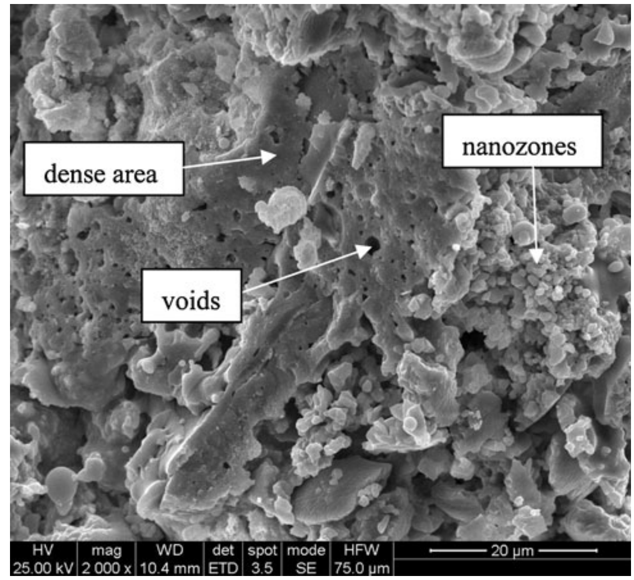

Fig. 2 SEM micrograph of the fracture surface of the nanostructured 4AlYSZ coating

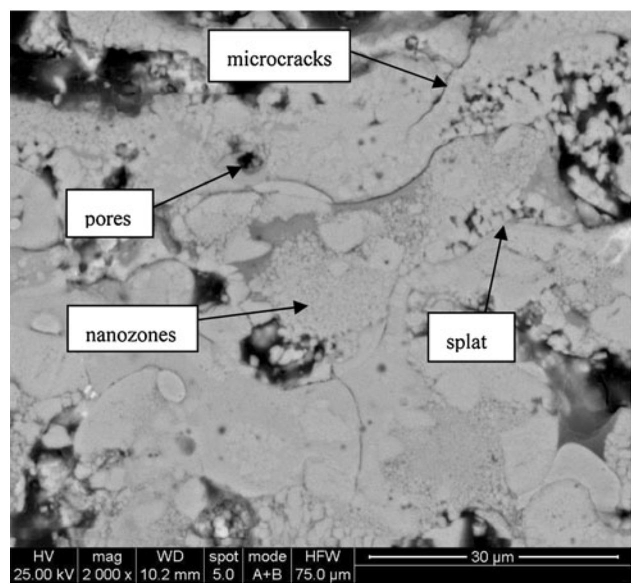

Fig. 3 The polished cross section of as-sprayed nanostructured 4AlYSZ

nanostructured 4AlYSZcoating. And the average grain size of the coating is about 65-70 nm.

3.3 Thermal Conductivity

The variation in thermal diffusivity as a function of temperature is shown in Fig. 5. The diffusivity decreases with the increasing temperature, as shown in Fig. 5. In the temperature range between room temperature and 600 °C, the diffusivity significantly decreases, and at

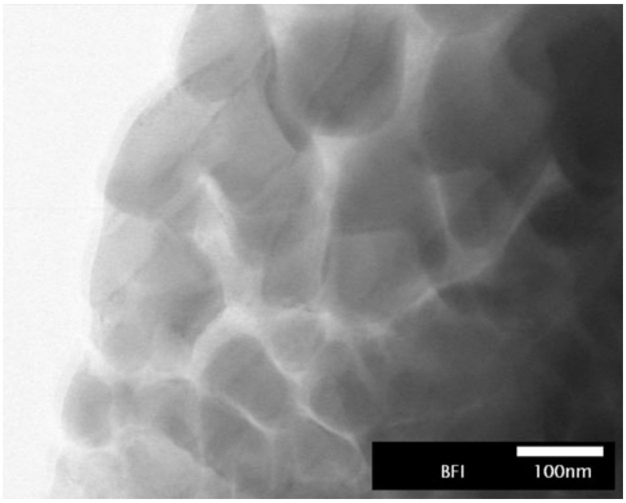

Fig. 4 TEM image of as-sprayed nanostrucutured 4AlYSZ coating

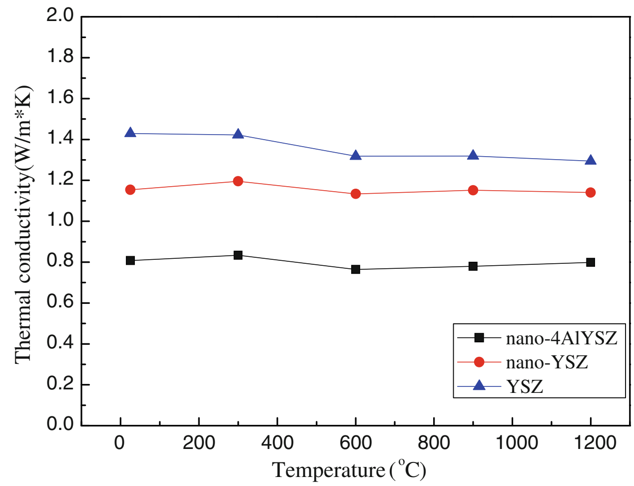

Fig. 6 Thermal conductivity of as-sprayed nano-4 AlYSZ coating, nanostructured and traditional YSZ coating as a function of temperature

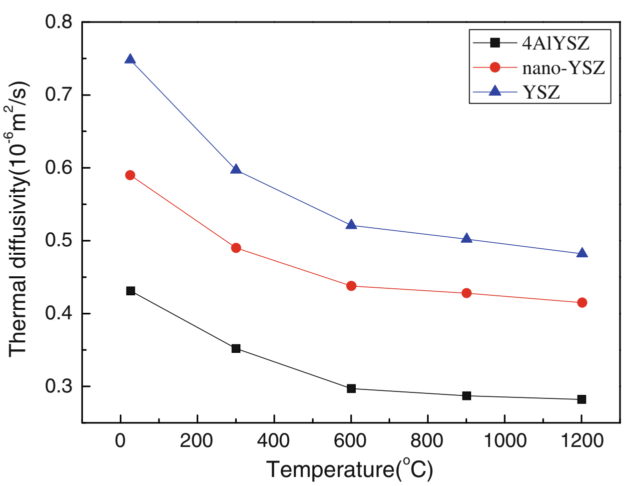

Fig. 5 Thermal diffusivity of as-sprayed nano-4AlYSZ coating, nanostructured and traditional YSZ coating as a function of temperature

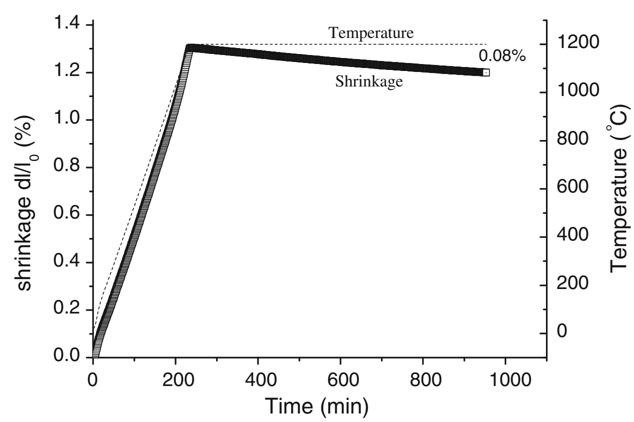

Fig. 7 Sintering behavior of the as-sprayed nanostructured 4AlYSZ coating at the 1200 °C for 12 h

higher temperatures from 600 to 1200 °C the diffusivity decreases very slightly. And from Fig. 5, the thermal diffusivity of nano-4AlYSZ coating is lower than that of traditional and nano-YSZ coating. The 4AlYSZ coating has the lowest thermal diffusivity.

The thermal conductivity was calculated using Eq 1, based on the measured thermal diffusivity, as shown in Fig. 6. The conductivity is about 0.81, 1.15 and 1.43 W/(m K) at room temperature corresponding to nano-4AlYSZ, nano-YSZ and traditional YSZ coating, respectively. The conductivity measured at 1200 °C is a little increase; this rise in conductivity is due to the starting sintering of the unmelted particles and pores during the flash measurement. The 4AlYSZ has the lowest thermal conductivity while the traditional YSZ coating has the highest.

3.4 Sintering and Thermal Cycling Life

Figure 7 is the sintering behavior of as-sprayed nanostructured AlYSZ coating at 1200 °C for 12 h. It is shown in Fig. 7 that the sintering rates of the nanostructured 4AlYSZ coating keeps as a constant for long sintering times. After heat treatment at 1200 °C for 12 h, the sintering shrinkage of nano-4AlYSZ coating is 0.08%. According to the results by Friedrich et al. (Ref 32) and our group (Ref 33), the sintering shrinkage of traditional YSZ after heat treatment at 1300 °C for about 12 h, is 0.13%, and the sintering shrinkage of nano-YSZ after heat treatment at 1250 °C for about 10 h coating is 0.22%. As discussed in Ref 11, the addition of Al_2O_3 improves the sintering resistance of the YSZ coatings.

Figure 8 presents the furnace cycling life of the coatings at 1100 °C where each result is the average of four measurements. Before 765 cycles, the nanostructured 4AlYSZ coating kept its integrity with no spallation occurred. After 765 cycles, a small spallation was observed at

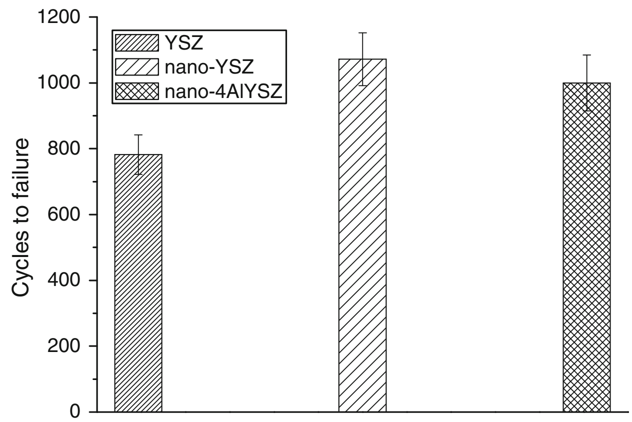

Fig. 8 Thermal cyclic life of nanostructured 4AlYSZ coating, nanostructured and conventional YSZ coating at 1100 °C

the coating edge, and after 1000 cycles the spallation extended to 5% area of the coating. The cycling life of the nano-4AlYSZ coating is about 1000 times, which is almost the same as that of nano-YSZ coating (1072 times). However, the cycling life of the nano-4AlYSZ coating is still much higher than that of traditional YSZ coating. The nanostructured 4AlYSZ coating has a longer thermal cycling life than that of conventional YSZ coating. Usually, nano-coatings tend to have a high porosity which is helpful to release thermal stresses and improve the strain tolerance.

4. Discussions

From Fig. 6 the thermal conductivity of the plasma-sprayed nanostructured 4AlYSZ coating is lower than that of the nanostructured and traditional YSZ coating. It was studied in our previous work (Ref 34) that the nanostructured YSZ had a lower thermal conductivity than that of traditional YSZ coating. After the addition of Al_2O_3, stronger phonon scattering tends to reduce the thermal transfer ability.

The phonons mean free path can be approximately described by

$$\frac{1}{l}=\frac{1}{l_i}+\frac{1}{l_p}+\frac{1}{l_b} \quad \text{(Eq 5)}$$

where l_i, l_p, and l_b are the phonon mean free paths due to intrinsic conductivity, point defect scattering, and grain-boundary scattering, respectively (Ref 35). Of these factors, the phonon mean free path is affected strongly by point defect scattering and l_p can be described in the following equation (Ref 36):

$$\frac{1}{l_p}=\frac{\alpha^3}{4\pi v^4}\omega^4 c\left(\frac{\Delta M}{M}\right)^2 \quad \text{(Eq 6)}$$

where α^3 is the volume per atom, v the transverse wave speed, ω the phonon frequency, c the defect concentration per atom, M the average mass of the host atom, ΔM is the average atomic mass difference between the solute (Y, Al) and host atom (Zr). And the grain-boundary scattering also provide a significant effect in nanostructured coatings as follows (Ref 37):

$$\frac{1}{l_b}=\frac{T\gamma^2}{20T_m\alpha} \quad \text{(Eq 7)}$$

where T_m is the absolute melting temperature, α is the lattice constant, and γ is the Gruneisen constant. Using this relation, l_b for single crystal YSZ is calculated to equal 25 nm at 300 K.

The added Al_2O_3 greatly decreased the thermal conductivity of nano-YSZ coating. Firstly, after plasma spraying Al_2O_3 is dissolved in ZrO_2, the ZrO_2 lattice is distorted and the concentration (c) of oxygen vacancy in 4AlYSZ is much higher than that in 8YSZ. The Al_2O_3 is dissolved in ZrO_2 in a substitutional way, because it is obviously impossible for it to be interstitially dissolved when considering the relative radius of Al^{3+} with respect to interstices in ZrO_2 lattice. Then the defect chemistry equation for Al_2O_3 can be written as

$$Al_2O_3 \rightarrow 2Al'_{Z_r} + V_{O^{\cdot\cdot}} + 3O_O^{\times}$$

Thus the predominant defects in the specimen should be $V_{O^{\cdot\cdot}}$ and Al'_{Z_r}. Al'_{Z_r} has a strong tendency to form defect associates with $V_{O^{\cdot\cdot}}$, when the concentration of Al'_{Z_r} is high, the association tendency is enhanced. After dissolving Al_2O_3 in the zirconia matrix additional oxygen vacancies are introduced to maintain the electrical neutrality of the lattice in the same manner as Y_2O_3 doping (Ref 38). The lattice distortion can effectively attenuate and scatter lattice phonon waves, lowering the thermal transfer.

Moreover, the atom masses of Al, Y and Zr are 26.98, 88.9 and 91.2, respectively, the average atomic mass difference ($|\Delta M|$) between the solute (Al) and host atom (Zr) is larger than that between Y and Zr, which contributes to higher effective phonon scattering by Al solute cations in 4AlYSZ than that of 8YSZ. Therefore, the reduction in thermal conductivity of 4AlYSZ is more obvious than that in YSZ.

The grain size of the nanostructured 4AlYSZ coating and YSZ coating is about 65 and 57 nm, which are comparable to the phonons mean free path (~25 nm) caused by grain boundary scattering. The small grain size in the nano-4AlYSZ and YSZ coatings contribute to the overall reduction of the thermal conductivity, due to the boundary thermal resistance promoted by the phonon scattering at grain boundaries (Ref 38). The micropores in the nanostructured 4AlYSZ and YSZ coatings are smaller in size and more homogeneously distributed with the porosity at the same level (Ref 11, 34) compared to the traditional YSZ coatings, and the splats in the nanostructured coatings are thinner, as compared to the conventional coatings. The smaller the micropores are, the more interfaces are produced, and the effect on the phonon scattering is strengthened, resulting in the reduction of thermal conductivity (Ref 39). To sum up, point defect scattering and grain-boundary scattering play a synergistic effect in reducing the thermal conductivity.

5. Conclusions

Effects of nano-Al_2O_3 addition on the microstructure, the thermal conductivity and thermal cycle life of nanostructured YSZ coating produced by APS are investigated. The conclusions are summarized as follows: The as-sprayed nanostructured AlYSZ coatings consist mainly of t-ZrO_2. The APS 4AlYSZ coating is characterized by nanozones, dense area, voids. After the addition of Al_2O_3, the thermal conductivity is decreased to 0.81 W/(m K) at room temperature, which is caused by the point defect and grain boundary phonon scattering. The lifetime of nanostructured 4AlYSZ coating is about 1000 cycles at 1100 °C, which is almost the same as that of nano YSZ coating. After sintering at 1200 °C for 12 h, the sintering shrinkage of the nano-4AlYSZ is about 0.08%.

Acknowledgments

This work is supported by the National Natural Science Foundation of China, the Aviation Science Foundation of 2008ZE51073, the Program for New Century Excellent Talents in University (NCET) and the Innovation Foundation of BUAA for PhD Graduates.

References

1. Y. Zeng, S.W. Lee, L. Gao, and C.X. Ding, Atmospheric Plasma Sprayed Coatings of Nanostructured Zirconia, *J. Eur. Ceram. Soc.*, 2002, **22**, p 347-351
2. R.S. Lima, A. Kucuk, and C.C. Berndt, Evaluation of Microhardness and Elastic Modulus of Thermally Sprayed Nanostructured Zirconia Coatings, *Surf. Coat. Technol.*, 2001, **135**, p 166-172
3. H. Chen, X.M. Zhou, and C.X. Ding, Investigation of the Thermomechanical Properties of a Plasma-Sprayed Nanostructured Zirconia Coating, *J. Eur. Ceram. Soc.*, 2003, **23**, p 1449-1455
4. A.L. Vasiliev, N.P. Padture, and X.Q. Ma, Coatings of Metastable Ceramics Deposited by Solution-Precursor Plasma Spray: I. Binary ZrO_2-Al_2O_3 System, *Acta Mater.*, 2006, **54**, p 4913-4920
5. A.L. Vasiliev and N.P. Padture, Coatings of Metastable Ceramics Deposited by Solution-Precursor Plasma Spray: II. Ternary ZrO_2-Y_2O_3-Al_2O_3 System, *Acta Mater.*, 2006, **54**, p 4921-4928
6. B. Liang, H.L. Liao, C.X. Ding, and C. Coddet, Nanostructured Zirconia-30 vol.% Alumina Composite Coatings Deposited by Atmospheric Plasma Spraying, *Thin Solid Films*, 2005, **484**, p 225-231
7. R.S. Lima and B.R. Marple, Nanostructured YSZ Thermal Barrier Coatings Engineered to Counteract Sintering Effects, *Mater. Sci. Eng. A*, 2008, **485**, p 182-193
8. N. Wang, C.G. Zhou, S.K. Gong, and H.B. Xu, Heat Treatment of Nanostructured Thermal Barrier Coating, *Ceram. Int.*, 2007, **33**, p 1075-1081
9. R.W. Trice, Y.J. Su, J.R. Mawdsley, K.T. Faber, A.R.D. Arellano-López, H. Wang, and W.D. Porter, Effect of Heat Treatment on Phase Stability, Microstructure, and Thermal Conductivity of Plasma-Sprayed YSZ, *J. Mater. Sci.*, 2002, **37**, p 2359-2365
10. H.B. Guo, H.B. Xu, X.F. Bi, and S.K. Gong, Preparation of Al_2O_3-YSZ Composite Coating by EB-PVD, *Mater. Sci. Eng. A.*, 2002, **325**, p 389-393
11. Q.H. Yu, C.G. Zhou, H.Y. Zhang, and F. Zhao, Thermal Stability of Nanostructured 13 wt.%Al_2O_3-8 wt.%Y_2O_3-ZrO_2 Thermal Barrier Coatings, *J. Eur. Ceram. Soc.*, 2010, **30**, p 889-897
12. Y. Liu, Y.F. Gao, S.Y. Tao, X.M. Zhou, and H.J. Luo, La_2O_3-Modified YSZ Coatings: High-Temperature Stability and Improved Thermal Barrier Properties, *Surf. Coat. Technol.*, 2009, **203**, p 1014-1019
13. M. Matsumoto, N. Yamaguchi, and H. Matasubara, Low Thermal Conductivity and High Temperature Stability of ZrO_2-Y_2O_3-La_2O_3 Coatings Produced by Electron Beam PVD, *Scr. Mater.*, 2004, **50**, p 867-871
14. M. Matsumoto, T. Kato, N. Yamaguchi, D. Yokoe, and H. Matsubara, Thermal Conductivity and Thermal Cycle Life of La_2O_3 and HfO_2 Doped ZrO_2-Y_2O_3 Coatings Produced by EB-PVD, *Surf. Coat. Technol.*, 2009, **203**, p 2835-2840
15. F. Tarasi, M. Medraj, A. Dolatabadi, J.O. Berghaus, and C. Moreau, Effective Parameters in Axial Injection Suspension Plasma Spray Process of Alumina-Zirconia Ceramics, *J. Therm. Spray Technol.*, 2008, **17**(5-6), p 685-691
16. J.O. Berghaus, J.G. Legoux, C. Moreau, F. Tarasi, and T. Chráska, Mechanical and Thermal Transport Properties of Suspension Thermal-Sprayed Alumina-Zirconia Composite Coatings, *J. Therm. Spray Technol.*, 2008, **17**(1), p 91-104
17. D.Y. Chen, E.H. Jordan, and M. Gell, Microstructure of Suspension Plasma Spray and Air Plasma Spray Al_2O_3-ZrO_2 Composite Coatings, *J. Therm. Spray Technol.*, 2009, **18**(3), p 421-426
18. F. Tarasi, M. Medraj, A. Dolatabadi, J.O. Berghaus, and C. Moreau, Phase Formation and Transformation in Alumina/YSZ Nanocomposite Coating Deposited by Suspension Plasma Spray Process, *J. Therm. Spray Technol.*, 2010, **19**(4), p 787-795
19. M. Matsumoto, K. Aoyama, H. Matasubara, K. Takayama, T. Banno, Y. Kagiya, and Y. Sugita, Thermal Conductivity and Phase Stability of Plasma Sprayed ZrO_2-Y_2O_3-La_2O_3 Coatings, *Surf. Coat. Technol.*, 2005, **194**, p 31-35
20. W. Ma, D. Mack, J. Malzbender, R. Vaßen, and D. Stöver, Yb_2O_3 and Gd_2O_3 Doped Strontium Zirconate for Thermal Barrier Coatings, *J. Eur. Ceram. Soc.*, 2008, **28**, p 3071-3081
21. J.H. Yu, H.Y. Zhao, S.Y. Tao, X.M. Zhou, and C.X. Ding, Thermal Conductivity of Plasma Sprayed $Sm_2Zr_2O_7$ Coatings, *J. Eur. Ceram. Soc.*, 2010, **30**, p 799-804
22. Z.H. Xu, L.M. He, R.D. Mu, S.M. He, X.H. Zhong, and X.Q. Cao, Influence of the Deposition Energy on the Composition and Thermal Cycling Behavior of $La_2(Zr_{0.7}Ce_{0.3})_2O_7$ Coatings, *J. Eur. Ceram. Soc.*, 2009, **29**, p 1771-1779
23. K. An, K.S. Ravichandran, T.E. Dutton, and S.L. Semiatin, Microstructure, Texture, and Thermal Conductivity of Single-Layer and Multilayer Thermal Barrier Coatings of Y_2O_3-Stabilized ZrO_2 and Al_2O_3 Made by Physical Vapor Deposition, *J. Am. Ceram. Soc*, 1999, **82**(2), p 399-406
24. X.Q. Cao, R. Vassen, S. Schwartz, W. Jungen, F. Tietz, and D. StÖ ever, Spray-Drying of Ceramics for Plasma-Spray Coating, *J. Eur. Ceram. Soc.*, 2000, **20**, p 2433-2439
25. G. Bertrand, P. Roy, C. Filiatre, and C. Coddet, Spray-Dried Ceramic Powders: Aquantitative Correlation Between Slurry Characteristics and Shapes of the Granules, *Chem. Eng. Sci.*, 2005, **60**, p 95-102
26. W.J. Parker, R.J. Jenkins, C.P. Butler, and G.L. Abbott, Flash Method of Determining Thermal Diffusivity. Heat Capacity, and Thermal Conductivity, *J. Appl. Phys.*, 1961, **32**, p 1679-1684
27. S. Dosta, I.G. Cano, J.R. Miguel, and J.M. Guilemany, Production and Characterization of Metastable ZrO_2-Al_2O_3Coatings Obtained by APS + Quench, *J. Therm. Spray Technol.*, 2008, **17**(3), p 360-364
28. H.P. Klug, L.E. Alexander, X-ray Diffraction Procedures for Polystalline and Amorphous Materials, John Wiley & Sons, Inc., London, 1954, p 148–154
29. L.L. Shaw and D. Goberman, The Dependency of Microstructure and Properties of Nanostructured Coatings on Plasma Spray Conditions, *Surf. Coat. Technol.*, 2000, **130**, p 1-8
30. H. Zhou, B. He, J. Wang, and B.D. Sun, Nanostructured Yttria Stabilized Zirconia Coatings Deposited by Air Plasma Spraying, *Trans. Nonferrous Met. Soc. China*, 2007, **17**, p 389-393
31. S. Raghavan, H. Wang, R.B. Dinwiddie, W.D. Porter, and M.J. Mayo, The Effect of Grain Size, Porosity and Yttria Content on the Thermal Conductivity of Nanocrystalline Zirconia, *Scr. Mater.*, 1998, **39**, p 1119-1125

32. C. Friedrich, R. Gadow, and T. Schirmer, Lanthanum Hexaaluminate—A New Material for Atmospheric Plasma Spraying of Advanced Thermal Barrier Coatings, *J. Therm. Spray Technol.*, 2002, **37**, p 2359-2365
33. J. Wu, H.B. Guo, L. Zhou, L. Wang, and S.K. Gong, Microstructure and Thermal Properties of Plasma Sprayed Nanostructure YSZ Thermal Barrier Coatings, *J. Therm. Spray Technol.*, Revision
34. Q.H. Yu, R. Abdul, N. Wang, and C.G. Zhou, Thermal Properties of Plasma-Sprayed Thermal Barrier Coating with Nanostructure, *Ceram. Int.*, Under Review
35. P.G. Klemens, Theory of the Thermal Conductivity of Solids, *Thermal conductivity*, Vol 1, R.P. Tye, Ed., Academic Press, London and New York, 1969, p 2-65
36. P.G. Klemens, Phonon Scattering by Oxygen Vacancies in Ceramics, *Phys. B*, 1999, **263-264**, p 102-104
37. G. Soyez, J.A. Eastman, L.J. Thompson, G. Bai, P.M. Baldo, A.W. McCormick, R.J. DiMelfi, A.A. Elmustafa, M.F. Tambwe, and D.S. Stone, Grain-Size-Dependent Thermal Conductivity of Nanocrystalline Yttriastabilized Zirconia Films Grown by Metal-Organic Chemical Vapor Deposition, *Appl. Phys. Lett.*, 2000, **77**(8), p 1155-1157
38. X. Guo, Space-Charge Conduction in Yttria and Alumina Codoped-Zirconia, *Solid State Ionics*, 1997, **96**, p 247-254
39. H. Zhou, F. Li, J. Wang, and B.D. Sun, Microstructure Analyses and Thermophysical Properties of Nanostructured Thermal Barrier Coatings, *J. Coat. Technol. Res.*, 2009, **6**(3), p 383-390